

Nuclear structure and dynamics of exotic nuclei: a study of beta-delayed neutron emission in Lithium-9

Abstract

This article presents a compact theoretical and computational study of the structure and beta-delayed neutron emission of the neutron-rich nucleus ${}^9\text{Li}$. A connected framework was used, combining an effective shell-model benchmark for low-lying spectroscopy and Gamow-Teller feeding, a two-body ${}^8\text{Li}+n$ description of the bound structure, a halo or core-EFT-style fit to the near-threshold sector, and a daughter-state decay map for ${}^9\text{Be}$ leading to neutron emission. The bound-state sector reproduced the dominant low-energy observables, including a ground-state neutron binding energy near -4.06 MeV and a first excited-state gap near 2.69 MeV. The fitted EFT-style sector gave $E_{p3/2} = -4.059659$ MeV and $\Delta E = 2.690697$ MeV, while also predicting a larger rms radius for the less bound excited configuration. The shell-model benchmark supplied the principal $3/2^-$, $5/2^-$, and $1/2^-$ branches together with effective $B(\text{GT})$ strengths used in the decay calculation. The delayed-neutron spectrum reproduced the dominant low-energy neutron peak at about 0.68 MeV and the adopted total delayed-neutron probability $P_n = 0.508$. A daughter-state decay map showed that neutron emission is controlled mainly by the lowest unbound fed states in ${}^9\text{Be}$, especially the $5/2^-$ state at $E_x = 2.430$ MeV, while higher states populate the upper-energy tail. The continuum analysis also showed that detailed resonance extraction remains numerically delicate, so the strongest conclusions of the present work concern bound-state observables, feeding structure, daughter-state interpretation, and spectrum-level decay quantities. The study therefore provides a compact phenomenological baseline that helps bridge the gap between experimental observables and theoretical description in neutron-rich exotic nuclei.

Keywords: Exotic nuclei, Lithium-9, beta-delayed neutron emission, daughter-state feeding, halo effective field theory

Volume 10 Issue 1 - 2026

Nathan Moyo, Manyika Kabuswa Davy

Department of Physics, School of Natural and Applied Sciences, Mulungushi University, Zambia

Correspondence: Manyika Kabuswa Davy, Department of Physics, School of Natural and Applied Sciences, Mulungushi University, Zambia

Received: March 26, 2026 | **Published:** May 04, 2026

Introduction

Exotic nuclei provide a demanding test of nuclear theory because weak binding, threshold effects, continuum coupling, and unusual decay modes become especially important far from stability.¹⁻³ Among light neutron-rich systems, ${}^9\text{Li}$ is particularly interesting because it lies at the intersection of bound-state structure, weak decay, and unbound daughter-state dynamics.^{4,5} It is also structurally relevant to the broader physics of lithium isotopes and halo systems, where low separation energies and extended wave functions lead naturally to effective core-plus-neutron descriptions. In ${}^9\text{Li}$, beta-delayed neutron emission offers a direct way of probing both the structure of the parent and the properties of the daughter nucleus ${}^9\text{Be}$ above neutron threshold.⁶⁻⁸ The present article therefore treats the problem as a connected structure-and-decay question involving the parent nucleus, the fed daughter states, and the emitted neutron spectrum. Rather than using one isolated model, a linked framework is adopted in which shell-model ideas, a two-body ${}^8\text{Li}+n$ description, a halo or core-EFT-style treatment of the near-threshold bound sector, and a daughter-state decay map all contribute to the final interpretation. The principal objective is to reproduce the main low-energy observables and then explain them physically in terms of parent structure, daughter feeding, and continuum neutron emission.

Motivation

The motivation for this study is to help bridge the gap between experimental observations and theoretical description in neutron-rich exotic nuclei. In the case of ${}^9\text{Li}$, experiments provide important observables such as binding energies, excitation energies, delayed-neutron probabilities, and neutron spectra, but a complete

interpretation requires a framework able to connect nuclear structure, daughter-state feeding, and continuum decay in a consistent way.^{9,10} A further motivation was the need to understand not only what the principal observables are, but why they take the values they do: why the dominant low-energy neutron peak appears near 0.68 MeV, which daughter states are responsible for it, and how the low-energy structure of ${}^9\text{Li}$ controls the decay.¹¹⁻¹⁵ This led to the construction of a connected workflow in which spectroscopy, radial structure, low-energy effective fitting, and daughter-state neutron-emission channels are treated as parts of the same physical problem rather than as unrelated calculations.¹⁶

Theoretical models

The theoretical description used in this work combines four related sectors. The first is an effective shell-model benchmark, introduced to represent the low-lying many-body structure and the transition pattern relevant to beta decay. The second is a two-body ${}^8\text{Li}+n$ model used to describe the dominant low-energy bound structure of ${}^9\text{Li}$. The third is a halo or core-EFT-style realization of the same near-threshold sector in terms of regulated short-range couplings.¹⁵ The fourth is a daughter-state decay model for ${}^9\text{Be}$, used to map fed states above neutron threshold into neutron-emission branches and final spectral contributions.

An effective shell-model benchmark was used to organize the low-lying many-body structure and the transition pattern relevant to the decay. The Hamiltonian is written as $H_{sm} = H_0 + V_{res}$

where H_0 contains the single-particle energies and V_{res} is the residual interaction. In matrix form, $H_{ij} = \epsilon_i \delta_{ij} + V_{ij}$. Diagonalization gives the mixed states $\Psi(\alpha)$ and the excitation energies $E_x(\alpha) = E\alpha -$

E0. Effective Gamow-Teller feeding is represented through $B\alpha(GT)\alpha \left| \langle \Psi_f^{(\alpha)} \parallel \hat{O}_{GT} \parallel \Psi_i \rangle \right|^2 > 2$

Here, the $B(GT)\alpha$ is the Gamow-teller transition strength to the daughter state α , Ψ_i is the initial parent-state wavefunction, $\Psi_f^{(\alpha)}$ is the final daughter-state wavefunction, and \hat{O}_{GT} is the Gamow-teller operator. The squared reduced matrix element therefore determines the effective transition strength into daughter states.

The shell-model sector therefore provides two essential ingredients: the excitation ladder used to organize the fed daughter states and the effective transition strengths that weight the beta feeding into those states.

The low-energy bound structure of ${}^9\text{Li}$ was then described in a two-body ${}^8\text{Li}+n$ picture. With reduced mass $\mu = \frac{m_n m_c}{m_n + m_c}$

The radial Schrödinger equation for the reduced wavefunction $u_j(r)$ is
$$\left[-\frac{\hbar^2}{2\mu} \frac{d^2}{dr^2} + \frac{\hbar^2(I+1)}{2\mu r^2} + V_{eff}(r) \right] u_j = E u_j(r)$$

In this equation, the reduced mass is $\mu = \frac{m_n m_c}{m_n + m_c}$, the centrifugal

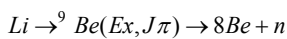
term contains the orbital angular momentum l , and $V_{eff}(r)$ represents the effective neutron-core interaction. The corresponding normalized wavefunctions are used to compute rms radii, densities, and low-energy phase behavior.

A halo or core-EFT-style description of the same near-threshold sector was introduced by replacing the short-range interaction with regulated low-energy couplings. The effective Hamiltonian is

$$H_{EFT} = -\frac{\hbar^2}{2\mu} \nabla^2 + V_{short}(r) + V_{cent}(r)$$

In this expression, H_{EFT} is the effective low-energy Hamiltonian of the core-neutron system, μ is the reduced mass, $V_{short}(r)$ represents the centrifugal contribution. The detailed short-distance structure is absorbed into the couplings C_{ij} , while $f_1(r; R_c)$ serves as a regulator function with scale R_c . In the p-wave sector a Gaussian-regulated form was used so that the low-energy couplings could be fitted directly to the ground-state binding and the first excited-state gap. This produces a more systematic low-energy interpretation of the same ${}^8\text{Li}+n$ structure.

For β -delayed neutron emission the decay chain was treated as



The neutron branch shapes were built with the penetrability. The penetrability introduces the correct threshold and angular-momentum dependence into the decay model. Each active branch is then assigned a width-like factor and a normalized line shape, and the full spectrum is obtained as the weighted sum over all fed daughter states and open neutron channels.

$$n(E) = \sum_i \sum_c W_{\beta, i} \omega_{ic} \phi_{ic}(E)$$

Here, $S_n(E)$ is the delayed-neutron spectrum at neutron energy E , $W_{\beta, i}$ is the beta-feeding weight into daughter state i , ω_{ic} is the branching fraction for channel c from that state, and $\phi_{ic}(E)$ is the normalized neutron-emission line shape for the corresponding branch. This equation shows that the total spectrum is obtained by summing

the weighted contributions of all fed states and all open neutron-emission channels.

Methodology

The computational procedure followed the same structure as the theoretical model. First, the shell-model benchmark Hamiltonian was diagonalized to produce the principal low-lying states and their effective $B(GT)$ strengths. These results were stored as the spectroscopy and feeding input for the later decay calculation. Second, the two-body ${}^8\text{Li}+n$ Hamiltonian was solved on a finite radial grid. The kinetic-energy operator, centrifugal term, and effective interaction were assembled into a radial Hamiltonian matrix, which was diagonalized numerically to obtain bound-state eigenvalues and eigenvectors. The reduced radial wavefunctions were then normalized by numerical integration, and rms radii were extracted from the expectation value of r^2 . Third, an EFT-style fit was performed in the $p_{3/2}$ and $p_{1/2}$ channels. For a fixed regulator scale, trial couplings were scanned over a chosen parameter range, the corresponding Hamiltonian was diagonalized, and the shallowest bound state in each channel was identified. The best couplings were then selected by minimizing the deviation from the adopted target values for the ground-state binding and the first excited-state gap. Once the fit was complete, the same couplings were used to generate bound-state radii and low-energy phase shifts. Fourth, the daughter-state decay calculation was built from the fed states of ${}^9\text{Be}$. For each state, the excitation energy relative to threshold, effective $B(GT)$, available branch centroids, partial waves, and reduced-width-like parameters were specified. The beta-decay phase-space factor was evaluated numerically, each neutron branch was assigned a penetrability-modified line shape, and all active branches were summed to form the final neutron spectrum. The total spectrum was normalized to the adopted delayed-neutron probability $P_n=0.508$. Finally, state-by-state and channel-by-channel decay maps were extracted so that the observed neutron spectrum could be interpreted directly in terms of the daughter states that produced it.

Results and data analysis

The bound-state sector reproduced the principal calibration observables of ${}^9\text{Li}$ with very high accuracy. In the EFT-style fit, the $p_{3/2}$ ground-state energy was obtained as -4.059659 MeV compared with the target -4.060000 MeV, while the first excited-state gap was 2.690697 MeV compared with the target 2.691000 MeV. The corresponding deviations were of order 10^{-4} MeV, showing that the fitted core-plus-neutron sector captures the dominant low-energy structure extremely well. The rms radii were 3.493073 fm for the $p_{3/2}$ state and 4.249610 fm for the $p_{1/2}$ state, consistent with the greater spatial extension of the less bound excited configuration. The shell-model benchmark produced an effective low-lying state ladder consisting of the $3/2^-$ ground state together with low, mid, and high $5/2^-$ branches and a low $1/2^-$ branch. The corresponding effective $B(GT)$ strengths were 0.0545 , 0.0492 , 0.0123 , 0.0518 , and 9.6931 for the principal branches used in the decay calculation. The delayed-neutron spectrum reproduced the dominant low-energy peak at 0.683020 MeV and the adopted total delayed-neutron probability $P_n=0.508000$. The energy-window decomposition showed that the decay is overwhelmingly concentrated below 2 MeV, where about 94.89% of the total strength resides, while the remaining windows carry only a small fraction of the decay yield. The daughter-state decay map completed the physical interpretation. It showed that the ${}^9\text{Be}$ ground state lies below neutron threshold and is therefore inactive for delayed-neutron emission. By contrast, the low $5/2^-$ state at $E_x=2.430$ MeV lies 0.765 MeV above

threshold and provides the dominant contribution to the spectrum, particularly through the observed 682 keV p-wave branch. The low $1/2^-$ state at $E_x=2.780$ MeV gives a secondary contribution, whereas the higher $5/2^-$ states mainly populate the upper-energy tail. The continuum analysis also revealed that although candidate resonance-like structures can be identified numerically, their detailed extraction remains sensitive to the box size and scan conditions. Consequently, the most reliable conclusions of the present work concern the bound-state observables, the daughter-state feeding structure, the daughter-side decay map, and the integrated spectrum quantities rather than a final detailed resonance catalogue.

Key numerical observables

Observable	Value
$E_{p3/2}$	-4.059659 MeV
ΔE	2.690697 MeV
$r_{rms(p3/2)}$	3.493073 fm
$r_{rms(p1/2)}$	4.249610 fm
Peak energy	0.683020 MeV
P_n	0.508000

Daughter-state decay map

State	Ex-Sn	Interpretation
3/2- ground	-1.665 MeV	bound; no n branch
5/2- low, 2.430	0.765 MeV	dominant source of 0.68 MeV peak
1/2- low, 2.780	1.115 MeV	secondary low-energy branch
5/2- mid, 7.940	6.275 MeV	feeds 6-8 MeV tail
5/2- high, 11.810	10.145 MeV	feeds upper-energy tail

Discussion

The combined results show that the different sectors of the framework play complementary roles. The shell-model benchmark supplies the many-body feeding structure that identifies which daughter states are populated and how strongly they are fed in β decay. The two-body and halo/core-EFT-style sectors then provide the low-energy structure interpretation of the parent nucleus in terms of the ${}^8\text{Li}+n$ system. In practice, this division of roles is important because no single simplified model is sufficient by itself to explain all of the observables. The shell-model benchmark alone does not provide the most accurate near-threshold bound-state calibration, while the low-energy core-plus-neutron description alone does not generate the many-body feeding pattern. The present study shows that a connected approach is therefore the most useful one for the ${}^9\text{Li}$ problem.

The daughter-side analysis is particularly significant because it completes the physical interpretation of the decay. The calculated daughter-state decay map shows that the ground state of ${}^9\text{Be}$ is neutron bound and therefore inactive for β -delayed neutron emission. The first important active state is the low $5/2^-$ branch at $E_x=2.430$ MeV, which lies 0.765 MeV above threshold and dominates the neutron output, especially through the observed branch near 0.682 MeV. The low $1/2^-$ state at $E_x=2.780$ MeV provides a smaller but still visible contribution, while the higher $5/2^-$ states mainly populate the upper-energy tail. This means that the main observed neutron spectrum is not controlled by many widely distributed daughter states, but mainly by the lowest unbound fed states of ${}^9\text{Be}$.

The spectrum-level observables are considerably more stable than the detailed continuum resonance assignments. The calculations reproduce the dominant low-energy neutron peak and the total delayed-neutron probability very well, and the energy-window

analysis shows that almost all of the strength is concentrated below 2 MeV. By contrast, the detailed resonance extraction remains more sensitive to numerical box size and scan conditions. The correct interpretation is therefore that the present framework is already strong in the sectors that matter most for the principal observables, namely the bound-state calibration, daughter feeding, threshold placement, and integrated spectral behavior. The resonance catalogue itself should still be regarded as provisional.

From a broader perspective, the present results show that the structure and decay of ${}^9\text{Li}$ can be described coherently once the parent nucleus, daughter nucleus, and emitted neutron are treated as parts of one linked problem. The success of the framework in reproducing the binding energy, excitation gap, peak energy, and adopted P_n indicates that the main low-energy physics is already well constrained. This provides a valuable phenomenological baseline for future work, including more systematic EFT developments, improved daughter-side resonance calculations, and more refined continuum analyses.

Conclusion

In summary, the combined shell-model, two-body, halo and core-EFT-style, and daughter-state decay framework provides a coherent description of the principal low-energy structure and decay observables of ${}^9\text{Li}$. The study reproduces the ground-state binding energy, the first excited-state gap, the dominant delayed-neutron peak, and the total P_n while also identifying the daughter states that control the neutron output. The strongest physical conclusion is that β -delayed neutron emission in ${}^9\text{Li}$ is governed mainly by the lowest unbound fed states of ${}^9\text{Be}$, especially the $5/2^-$ state at 2.430 MeV. The work therefore offers a compact phenomenological baseline for interpreting ${}^9\text{Li}$ and for future refinements of the continuum and resonance sectors.

Acknowledgments

None.

Conflicts of interest

The authors declares that there are no conflicts of interest.

References

- Bjornstad T. Systematics of energy levels in light nuclei. *Nucl Phys A*. 1981;359:1–23.
- George L, Davy MK. The Coleman-Weinberg potential and its application to the hierarchy problem. *Phys Astron Int J*. 2023;7(2):104–107.
- Nyman G. *Nucl Phys A*. 1990;510:189.
- Davy MK, Xiao BW. D meson decays and new physics. *J Phys Astron*. 2017;5(1):110.
- Prezado Y. *Nucl Phys A*. 2004;746:518c.
- Davy MK, Levy MK. On the radiation of gluon jets: A summary. *Int J Sci Eng Inv*. 2019;5(6):2455–4286.
- Tilley DR. *Nucl Phys A*. 2004;745:155.
- Judith K, Manyika DK. Gluon jets evolution in the quest for new physics. *Phys Astron Int J*. 2023;7(2):109–111.
- Kelley JH, Kwan E, Purcell JE, et al. Energy levels of light nuclei $A = 11$. *Nucl Phys A*. 2004;745:155–362.
- Ewald G. Observation of resonance structures in light nuclei via photon scattering. *Phys Rev Lett*. 2004;93:113002.
- Sanchez R. Measurement of nuclear structure effects in light exotic systems. *Phys Rev Lett*. 2006;96:033002.

12. Davy MK. The future of theoretical particle physics: A summary. *J Phys Astron*. 2017;5(1):109.
13. Dangtip S. *Nucl Phys A*. 2000;677:3.
14. Riisager K. *Phys Scr*. 2013;T152:014001.
15. Michael M, Manyika KD. Prospects of the Higgs boson: An overview. *Phys Astron Int J*. 2024;8(2):127–131.
16. Lane AM, Thomas RG. *Rev Mod Phys*. 1958;30:257.